Triple quantum dot device designed for three spin qubits

ARTICLE *in* APPLIED PHYSICS LETTERS · DECEMBER 2010

Impact Factor: 3.3 · DOI: 10.1063/1.3518919 · Source: IEEE Xplore

Triple quantum dot device designed for three spin qubits

T. Takakura,[1,a)] M. Pioro-Ladrière,[2] T. Obata,[1] Y.-S. Shin,[3] R. Brunner,[4] K. Yoshida,[1] T. Taniyama,[5] and S. Tarucha[1]
[1]*Department of Applied Physics, The University of Tokyo, Tokyo 113-8656, Japan*
[2]*Département de Physique, Université de Sherbrooke, Quebec J1K 2R1, Canada*
[3]*Department of Materials Science and Engineering, Pohang University of Science and Technology, Gyeongsangbuk-do 790-784, Republic of Korea*
[4]*Institute of Physics, University of Leoben, Styria A-8700, Austria*
[5]*Materials and Structures Laboratory, Tokyo Institute of Technology, Kanagawa 226-8503, Japan and PRESTO, Japan Science and Technology Agency, Saitama 332-0012, Japan*

(Received 4 August 2010; accepted 29 October 2010; published online 23 November 2010)

Electron spin confined in quantum dots is a promising candidate for experimental qubits. Aiming at realizing a three spin-qubit system, we designed split micromagnets suitable for the lateral triple quantum dots. From numerical simulations of the stray magnetic field distribution, field gradients ~ 0.8 T/μm and differences of *in-plane* components ~ 10 mT can be attained, which enable the electrical and addressable manipulation of three qubits. Furthermore, this technique can be applied for up to 25 qubits in realistic multiple quantum dots. For the first step of implementing such three-qubit systems, a relevant triple quantum dot device has been fabricated and characteristic charge states were observed. © *2010 American Institute of Physics*. [doi:10.1063/1.3518919]

Since the proposal of electron-spin-based quantum computation,[1] many experimental challenges have been addressed to coherently manipulate electron spins in quantum dots (QDs). Electron spin resonance (ESR) is the fundamental tool for electron spin qubits. ESR usually requires a dc and an ac magnetic field normal to each other. The ac field frequency matches the Zeeman energy imposed by the dc field. Manipulation of single electron spins can be achieved by making the ac field local to a QD in the presence of a global static magnetic field. Several ESR experiments have been demonstrated by generating such an ac field in various ways: ac current injection into an on-chip coil[2] and conversion from ac voltage via spin-orbit interaction.[3]

However, in order to handle individual electron spins in multiple QDs or to make multiqubit systems, it is necessary to establish the ESR condition of both dc and ac magnetic fields local to each QD. We have recently proposed and demonstrated a new technique of electrically driven single spin resonance (EDSR) using a micromagnet (MM) to facilitate such an ESR condition.[4,5] An ac magnetic field is effectively generated by electrical oscillation of an electron inside a QD under a gradient of the *out-of-plane* stray field, which is imposed by a MM located above. This MM also brings about an *in-plane* stray field local to each QD. This technique, therefore, allows us to address single spins in multiple QDs with EDSR at different resonance frequencies. This scheme has been demonstrated for two individual electrons in a double QD.[6]

The next step is to extend the above technique to triple QDs (TQDs) for manipulating three individual electrons. However, there are just a few previous reports on fabrication and characterization of TQDs holding few electrons,[7–9] and no report on TQDs designed for three spin qubits. In this work we propose a TQD arrangement and MM-geometries to optimize the stray magnetic field distribution across the three QDs such that three spin qubits can be independently addressed. Because our design requires in-line QDs, we propose a lateral TQD geometry that satisfies this demand. We then fabricated the TQD device and checked the proper operation of it by examining the charge stability diagrams with tunable numbers of electrons in each QD.

We have designed a split type MM placed above the surface gates, which define three dots in a row in a two-dimensional electron gas (2DEG). The overview is shown in Fig. 1(a). The distance between the two tapered-shape MMs, $s(x)$, varies linearly as a function of x. The QDs are positioned on the x axis or center of the two MMs. We assume that the external static magnetic field $\boldsymbol{B}_{\mathrm{ext}}$ is strong enough to magnetize the MMs along the y axis. A stray magnetic field is then produced in the out-of-plane ($B^M{}_z$) and in-plane ($B^M{}_y$) by the MMs. Figures 1(b) and 1(c) show the calculation of $B^M{}_z$, and $B^M{}_y$ at $x=0$, respectively, for a typical design of the MMs made of Co. A slanting magnetic field of $B^M{}_z$ is established in the y direction with the gradient $b_{\mathrm{sl}}=dB^M{}_z/dy$. This b_{sl} is of order T/μm. In addition, $B^M{}_y$ is maximal at $y=0$.

To realize EDSR for single electrons in the individual QDs, a microwave voltage is applied to a high-frequency gate electrode to oscillate the electron position in each QD in the y direction, so that the electrons are exposed to an effective ac magnetic field in the z direction.[4] When the microwave frequency f_{MW} is consistent with the Zeeman energy E_Z, i.e., $hf_{\mathrm{MW}}=E_Z$, where h is the Plank constant, Rabi oscillation or spin flip between the up-spin and down-spin state occurs with the frequency proportional to the amplitude of the ac magnetic field.

The Zeeman energy for each QD must be given by B_0, the sum of B_{ext} and $B^M{}_y$. Note that $B^M{}_z$ is averaged out since the QDs are at $y=0$. These B_0 are local to each QD, because $B^M{}_y$ depends on the position x. Figures 1(d) and 1(e) show the calculation of $B^M{}_y$ and b_{sl}, respectively, with offset of the QD position in the y direction as a parameter. Both $B^M{}_y$ and b_{sl} are maximal at $y=0$. The three dots are spaced by 150 nm, which is a typical value for real coupled QD devices. In Fig. 1(d) the values of $B^M{}_y$ are different by $\Delta B^M{}_y \sim 10$ mT

a)Electronic mail: takakura@meso.t.u-tokyo.ac.jp.

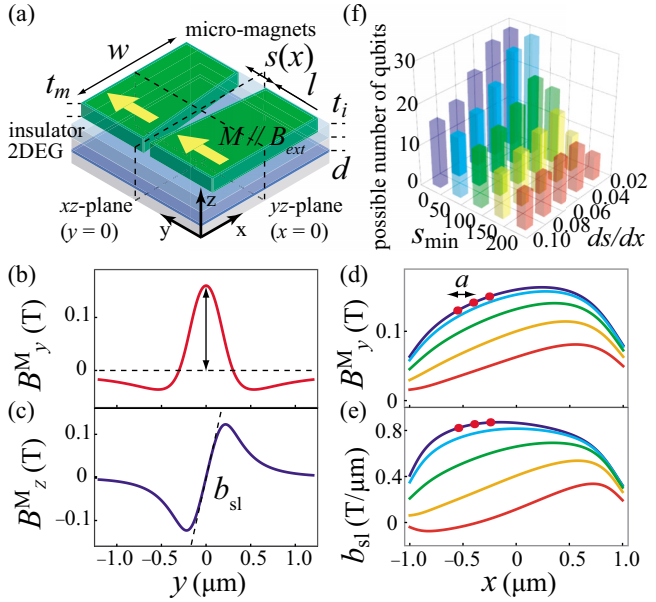

FIG. 1. (Color online) A possible design of MMs and numerical calculation of the stray magnetic field from MMs. (a) An aerial view of the TQD device integrated with ferromagnetic strips (trapezoids on top). The insulating layer lies between the MMs and the wafer surface. The thick arrows indicate the direction of the external magnetic field B_{ext} and magnetization M. The origin is fixed at the center of two MMs. (b) and (c) In-plane (B^M_y) and out-of-plane (B^M_z) profiles of the stray magnetic field produced by MMs along x =0, respectively. (d) and (e) Spatial distributions of B^M_y and $b_{sl}=dB^M_z/dy$ as a function of x position, respectively. Three circles in each figure indicate the position of QDs in our case, with interdot distance a equal to 150 nm obtained from the calculated electrostatic potential in Fig. 2(b). The five colored curves show B^M_y and b_{sl} for QDs offset in the y direction from 0 nm (top) to 200 nm (bottom) in steps of 50 nm. Dimensions l, w, d, t_m, and t_i are set to 5, 2, 0.10, 0.15, and 0.1 μm. Dimension s is linearly varied from 0.15 to 0.55 μm. (f) Achievable numbers of qubits as a function of ds/dx and s_{min}. We assume the EDSR conditions are such that the differences between neighboring QDs are larger than 3 mT and the strength of the slanting field at each QD is larger than 0.5 T/μm. Here dimensions a, l, w, d, t_m, and t_i are 0.15, 100, 14, 0.10, 0.25, and 0.05 μm. In all calculations the magnetization of ferromagnetic strips, $\mu_0 M$, is taken as 1.8 T which corresponds to that of Co.

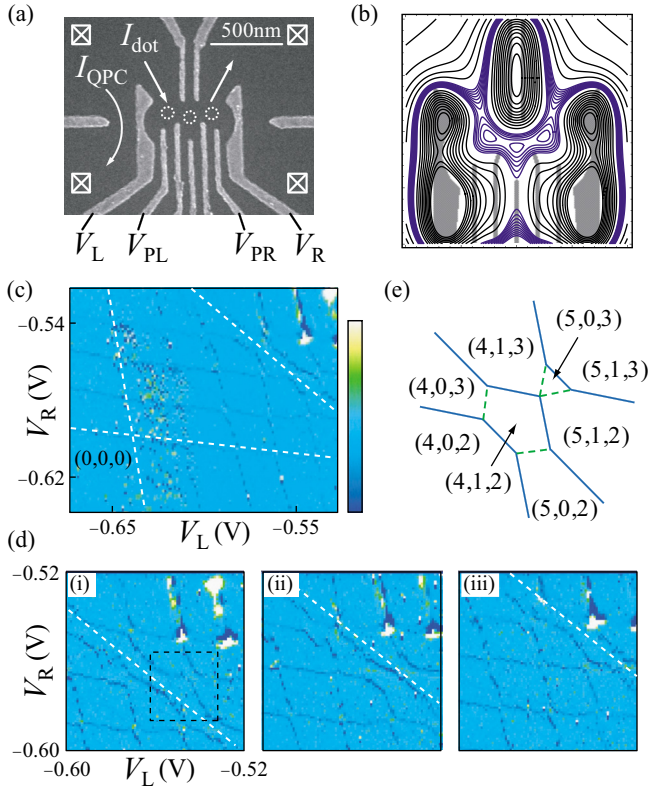

FIG. 2. (Color online) Lateral TQD device and the experimental results. (a) A scanning electron micrograph of the TQD device. White circles indicate the location of the QDs. Ohmic contacts are shown as boxes in the corners. White arrows outline the paths of current through the TQD and one of the QPC charge sensors. (b) A contour plot of electrostatic potential generated by the surface gates simulated in a 1 μm^2 region. The contours around the Fermi level are five times more precise than the others to emphasize the potential minima of QDs. (c) A charge stability diagram showing the few-electron regime measured with the charge sensor as a function of side-gate voltages. Dark lines signal the addition/removal of a single electron to the TQD. White dotted lines emphasize the charge transitions between 0 and 1 electron in each of QDs. A set of three indices (0,0,0) indicates that the TQD is empty there. (d) A series of zoomed-in diagrams of (b), but with varying V_{PL} and V_{PR} by 10 mV simultaneously. (e) Schematic of the charge configuration in the vicinity of the quadruple point [shown as the dashed square in Fig. 2(d)(i)] with sets of equilibrium charge numbers.

from QD to QD, resulting in the different f_{MW} by Δf_{MW} =56 MHz for GaAs QDs with a $|g|$-factor of 0.44. The Δf_{MW} is large enough to discriminate EDSR among the three QD although ESR peaks are broadened due to the fluctuating nuclear field of GaAs materials.[10,11] b_{sl} is approximately the same for the three dots, $b_{sl}\approx 0.8$ T/μm. We can estimate that the Rabi frequencies of these qubits are $\sim$10 MHz,[12] which leads to shorter π-pulse time than T_2^*, typically $\sim$100 ns.

We now discuss the permissible range of MM misalignment, which inevitably occurs in device fabrication. As the QDs move away from the center, both b_{sl} and ΔB^M_y decreases [Figs. 1(d) and 1(e)]. The permissible ranges in x and y directions to keep $b_{sl}>0.5$ T/μm and $\Delta B^M_y>10$ mT are $\sim\pm 100$ and $\sim\pm 50$ nm, respectively. These are within the accuracy of alignment in real device processing.

Next we estimate the number of qubits attainable with our designs. Important parameters are the width w of the MMs, the taper, ds/dx, and the minimum gap s_{min} [Fig. 1(a)]. Figure 1(f) shows the attainable number of qubits as a function of ds/dx and s_{min} for w=14 μm under the condition $\Delta B^M_y>3$ mT and $b_{sl}>0.5$ T/μm. The lower bound of ΔB^M_y is chosen to be consistent with the EDSR line width of B_{ext} measured before.[6,12] Our calculation shows that more than 25 qubits are achievable in simple tapered but carefully designed MMs.

Spin-orbit interaction (SOI) is another mechanism to provide an effective ac magnetic field.[3] By taking into account the SOI, the total field gradient is expressed as $b_{sl}^{total}=b_{sl}^M+2B_{ext}(l_\alpha^{-1}\pm l_\beta^{-1})$,[13] where b_{sl}^M is the field gradient imposed by MMs, l_α and l_β the Rashba and Dresselhaus spin-orbit length, respectively. Plus and minus signs are for [110] and [1$\bar{1}$0] directions, respectively, along which we oscillate electron spins. For the single MM case, b_{sl}^M is negative when we assume B_{ext} is positive.[6] On the other hand, for the split-type MM b_{sl}^M becomes positive and thus the Rashba term enhances the slanting field from MMs. We can fully utilize both Rashba and Dresselhaus contributions if we choose the [110] axis as an oscillatory direction (when l_α and $l_\beta>0$).

Based on the above, we have fabricated a relevant lateral TQD, in the first step, without MMs. Figure 2(a) shows a scanning electron micrograph of the device, specifically designed for in-line QDs [Fig. 2(b)]. The TQD is made in a

2DEG at a GaAs/AlGaAs heterointerface by Ti/Au (10 nm/20 nm) Schottky gates (bright regions). The 2DEG is 90 nm beneath the surface. The Schottky gates are designed to create three QDs in a row as shown in Fig. 1(a). Moreover, a capping gate is placed on top with a 100 nm thick insulating layer in between. This gate is negatively biased to reduce the carrier density and therefore the charge noise.[6,14]

All experiments were performed in a dilution refrigerator at the base temperature of ~10 mK. Initially we measured electron transport through the TQD to characterize the Coulomb blockade effect. Then we used two quantum point contacts (QPCs) near the TQD as charge sensors to derive the stability diagram of the charge states.[15] Here we measured the QPC current I_{QPC} as a function of two side-gate voltages V_L and V_R for the left and right QD, respectively, with plunger gate voltages V_{PL} and V_{PR} as parameters.

Figure 2(c) shows the measured charge stability diagram in the numerical derivative dI_{QPC}/dV_R versus $V_L - V_R$. Each dark line corresponds to a Coulomb peak or single electron charging of one of the three dots. Since each side gate is capacitively coupled to the three dots but by a different amount, the dark lines are classified into three families with different slopes. Almost vertical (horizontal) dark lines indicate the charging of the left (right) dot. A dark line with the slope of $dV_R/dV_L=-1$ is then assigned to the charging of the central dot. The exact electron numbers N_L, N_C, and N_R in the left, central, and right QD, respectively, are determined by counting the number of dark lines, starting from the state $(N_L,N_C,N_R)=(0,0,0)$ where all electrons are depleted in the TQD.

For any TQD, three independent variables are needed to fully control the charge states.[7–9] Therefore, the stability diagram should be considered in the three-dimensional phase space, where the charging of one QD is expressed by a plane and an intersection of three different planes for three QDs splits into four quadruple points.

In our TQD we could reach the empty configuration of the stability diagram [Fig. 2(c)], and tune independently the electron number in each QD. Here the combination of V_{PL} and V_{PR} [see Fig. 2(a)] is the third variable to tune the configuration of the central dot relative to the other dots [Fig. 2(d)]. Close inspection of the stability diagrams allows us to identify the quadruple points in the few-electron regime [Fig. 2(e)].

In conclusion, we have designed a split-type MM to enable multispin qubits in QDs. We have found by simulation that the proposed design is suitable for addressing up to 25 single electron spins. For the implementation with lateral QDs, we have fabricated a TQD that could reach the few-electron regime. We used a charge sensing technique to derive the stability diagrams of charge states, indicating that the three dot states can be independently controlled with the gate voltages. Our MM technique is useful not only for lateral QDs but also for other kinds, such as self-assembled QDs.

Part of this work is financially supported by JSPS Grant-in-Aid for Scientific Research S (Grant No. 19104007), MEXT Grant-in-Aid for Scientific Research on Innovative Areas (Grant No. 21102003), Special Coordination Funds for Promoting Science and Technology, Funding Program for World-Leading Innovative R and D on Science and Technology (FIRST), and DARPA QuEST Grant No. HR0011-09-1-0007. T.T. acknowledges the financial support from JSPS for the Research Fellowships. M.P.-L. acknowledges the National Sciences and Engineering Research Council (NSERC) and the Canadian Institute for Advanced Research (CIFAR) for financial support.

[1] D. Loss and D. P. DiVincenzo, Phys. Rev. A **57**, 120 (1998).
[2] F. H. L. Koppens, C. Buizert, K. J. Tielrooij, I. T. Vink, K. C. Nowack, T. Meunier, L. P. Kouwenhoven, and L. M. K. Vandersypen, Nature (London) **442**, 766 (2006).
[3] K. C. Nowack, F. H. L. Koppens, Yu. V. Nazarov, and L. M. K. Vandersypen, Science **318**, 1430 (2007).
[4] Y. Tokura, W. G. van der Wiel, T. Obata, and S. Tarucha, Phys. Rev. Lett. **96**, 047202 (2006).
[5] M. Pioro-Ladrière, Y. Tokura, T. Obata, T. Kubo, and S. Tarucha, Appl. Phys. Lett. **90**, 024105 (2007).
[6] M. Pioro-Ladrière, T. Obata, Y. Tokura, Y.-S. Shin, T. Kubo, K. Yoshida, T. Taniyama, and S. Tarucha, Nat. Phys. **4**, 776 (2008).
[7] D. Schröer, A. D. Greentree, L. Gaudreau, K. Eberl, L. C. L. Hollenberg, J. P. Kotthaus, and S. Ludwig, Phys. Rev. B **76**, 075306 (2007).
[8] L. Gaudreau, A. Kam, G. Granger, S. A. Studenikin, P. Zawadzki, and A. S. Sachrajda, Appl. Phys. Lett. **95**, 193101 (2009).
[9] S. Amaha, T. Hatano, T. Kubo, S. Teraoka, Y. Tokura, S. Tarucha, and D. G. Austing, Appl. Phys. Lett. **94**, 092103 (2009).
[10] A. C. Johnson, J. R. Petta, J. M. Taylor, A. Yacoby, M. D. Lukin, C. M. Marcus, M. P. Hanson, and A. C. Gossard, Nature (London) **435**, 925 (2005).
[11] F. H. L. Koppens, J. A. Folk, J. M. Elzerman, R. Hanson, L. H. Willems van Beveren, I. T. Vink, H. P. Tranitz, W. Wegscheider, L. P. Kouwenhoven, and L. M. K. Vandersypen, Science **309**, 1346 (2005).
[12] T. Obata, M. Pioro-Ladrière, Y. Tokura, Y.-S. Shin, T. Kubo, K. Yoshida, T. Taniyama, and S. Tarucha, Phys. Rev. B **81**, 085317 (2010).
[13] Y. Tokura (private communication).
[14] C. Buizert, F. H. L. Koppens, M. Pioro-Ladrière, H. P. Tranitz, I. T. Vink, S. Tarucha, W. Wegscheider, and L. M. K. Vandersypen, Phys. Rev. Lett. **101**, 226603 (2008).
[15] J. R. Petta, A. C. Johnson, C. M. Marcus, M. P. Hanson, and A. C. Gossard, Phys. Rev. Lett. **93**, 186802 (2004).